NanoImpact 27 (2022) 100414

Contents lists available at ScienceDirect

NanoImpact

journal homepage: www.elsevier.com/locate/nanoimpact

Airborne emissions from combustion of graphene nanoplatelet/epoxy composites and their cytotoxicity on lung cells *via* air-liquid interface cell exposure *in vitro*

Woranan Netkueakul [a,b,c], Savvina Chortarea [c], Kornphimol Kulthong [d], Hao Li [a,b], Guangyu Qiu [a,b], Milijana Jovic [e], Sabyasachi Gaan [e], Yvette Hannig [c], Tina Buerki-Thurnherr [c], Peter Wick [c,**], Jing Wang [a,b,*]

[a] Institute of Environmental Engineering, ETH Zurich 8093, Zurich, Switzerland
[b] Laboratory for Advanced Analytical Technologies, Empa, Swiss Federal Laboratories for Materials Science and Technology, 8600 Dübendorf, Switzerland
[c] Particles-Biology Interactions Lab, Empa, Swiss Federal Laboratories for Materials Science and Technology, 9014 St. Gallen, Switzerland
[d] National Nanotechnology Center (NANOTEC), National Science and Technology Development Agency (NSTDA), 12120 Pathum Thani, Thailand
[e] Additives and Chemistry Group, Advanced Fibers, Empa, Swiss Federal Laboratories for Materials Science and Technology, 9014 St. Gallen, Switzerland

ARTICLE INFO

Editor: Dr. Bernd Nowack

Keywords:
Graphene nanoplatelet
Nanofiller
Polymer combustion
Air-liquid interface
In vitro hazard assessment
Alveolar epithelium

ABSTRACT

Graphene nanoplatelet (GNP) as a nanofiller improves the mechanical strength, electrical conductivity, and flame retardancy of the polymers significantly. With an increasing number of GNP-reinforced products, a careful safety assessment is needed to avoid social and economic setbacks. However, no study has addressed the effects of combustion-generated emissions from GNP-reinforced products in the lung, the most sensitive exposure route to airborne particles. Therefore, we studied the influence of GNP as a nanofiller on the emitted particles and polycyclic aromatic hydrocarbons (PAHs), and cytotoxicity of the emissions from the combustion of pure epoxy (EP) and GNP-reinforced epoxy (EP-GNP). GNP was not detected in the airborne emissions. PAHs were found in airborne particles of both emissions from EP and EP-GNP, with some differences in their concentrations. A first hazard assessment was performed on human alveolar epithelial cells exposed to the airborne emissions at air-liquid interface conditions. At 24 h and 96 h after the exposure, similar responses were observed between EP and EP-GNP except an acute transient decrease in mitochondrial activity after exposure to the emissions from EP-GNP. Both emissions from EP and EP-GNP had no acute effects on membrane integrity, cell morphology or expression of anti-oxidative stress markers (*HMOX1* and *SOD2* genes). Meanwhile, both emissions induced the activation of the aryl hydrocarbon receptor (*CYP1A1* gene) and a transient (pro-) inflammatory response (MCP-1), but the effects between EP and EP-GNP were not significantly different.

1. Introduction

Graphene nanoplatelet (GNP) is a two-dimensional carbonaceous material consisting of a few to several layers of graphene sheets (Wick et al., 2014) GNP has been extensively studied and applied in commercial products as nanofillers to improve the mechanical, electrical, and fire performance of the polymers (Chandrasekaran et al., 2013; Zhang et al., 2018). Due to the improved properties of the composites, an increasing demand of graphene-related materials is predicted (Garrington, 2020; Reiss et al., 2019) and will raise the production volume of GNP and GNP-based products (Kong et al., 2019). Therefore, a careful assessment of the potential adverse health effects due to an increasing use of GNP in commercial products is essential.

One of the scenarios that can occur at the end-of-life of the GNP-reinforced polymers is the combustion process such as waste incineration, which features a nearly complete combustion in the controllable manner, or an accidental fire, which is likely an incomplete combustion that probably generates more soot. Combustion is a highly complex process, and it is even more challenging to fully understand the combustion of nanomaterial-embedded polymers. The combustion of epoxy

* Corresponding author at: Institute of Environmental Engineering, ETH Zurich 8093, Zurich, Switzerland.
** Corresponding author at: Swiss Federal Laboratories for Materials Science and Technology, 9014 St. Gallen, Switzerland.
E-mail address: jing.wang@ifu.baug.ethz.ch (J. Wang).

https://doi.org/10.1016/j.impact.2022.100414
Received 25 May 2022; Received in revised form 24 July 2022; Accepted 4 August 2022
Available online 9 August 2022

(EP) produces a large amount of soot and toxic gases such as CO and HCN (Dao et al., 2014). During the combustion, epoxy resin can be degraded by chain scission mechanism and further decomposed to light combustible gases such as allyl alcohol, acetone, and other hydrocarbons (Levchik and Weil, 2004). Rearrangement of the atoms and cyclization of the molecules can occur, which may lead to the char formation. GNP acts as a flame retardant when used as a nanofiller in different kinds of polymer (Dittrich et al., 2013; Liu et al., 2014; Zhang et al., 2018). Addition of GNP slows down the combustion of epoxy composite due to the barrier effect, attributed to a migration of GNP to the surface of the polymer to form a protective layer (Zhang et al., 2018). GNP could be transformed by thermal oxidation at high temperature during the combustion (Ermakov et al., 2015; Hahn, 2005). At a temperature over 850 °C, the defected and basal plane of graphitic layer can be etched leading to hole formation in the layer (Hahn, 2005). Moreover, GNP may be dislocated from the matrix during the combustion process and exist as a part of the char (Kotsilkov et al., 2018) and/or in an airborne form, which may pose an additional risk to humans and the environment.

Biological effects of GNP have been reported *in vitro* and *in vivo* in different biological systems (Drasler et al., 2018; Li et al., 2012; Netkueakul et al., 2020b; Park et al., 2017; Schinwald et al., 2012) and are summarized in several reports (Fadeel et al., 2018; Ou et al., 2016; Yang et al., 2013; Zhang et al., 2016). Due to its distinct platelet-like structure, Schinwald and coworkers showed that GNPs with a thickness of 100 nm and diameters up to 25 μm have an aerodynamic diameter in the respirable range (smaller than 4 μm) and could be deposited beyond the ciliated airway, in the alveolar structures where macrophages are mainly responsible for the clearance process (Schinwald et al., 2012). GNP with a diameter larger than 15 μm could not be entirely phagocytosed by macrophages and thus provoked frustrated phagocytosis, increase in inflammatory cytokines (at 1–10 μg/cm^2), and in a later state loss of cellular membrane integrity (only at 5 and 10 μg/cm^2). Our previous study showed that GNP with larger lateral dimension (25 μm) at the delivered doses of 20 and 40 μg/mL induced the release of lactate dehydrogenase due to membrane rupture in THP-1 macrophages, whereas the smaller GNP (5 μm) did not (Netkueakul et al., 2020b). On the other hand, Drasler et al. revealed that GNP with 1–2 μm lateral dimension at 0.3 and 1 μg/cm^2 exposure doses did not cause cytotoxic effects, (pro-) inflammation or oxidative stress in a 3D alveolar lung cell model (Drasler et al., 2018). Apart from a variation of the biological models in different studies, the physicochemical characteristics of GNP such as the lateral dimension, thickness, surface area, and surface chemistry could also play a crucial role in the toxicity of GNP (Ou et al., 2016; Yang et al., 2013), which may explain the inconsistency in the reported biological responses. Nevertheless, in the context of a combustion event, the toxicity of the pristine GNP may be of limited relevance since the released GNP (if any) likely undergoes transformation of its properties during composite fabrication and thermal decomposition. Moreover, the combination of epoxy and GNP could lead to the formation of new particle or gas emissions or induce synergistic effects.

Despite of the growing interests in applying GNP as nanofillers and the increasing number of GNP-filled polymer products on the market, little is known about the effects of GNP on the emissions from the combustion of GNP-containing nanocomposites and the potential hazard of the released particles and gases. Like GNP, carbon nanotube (CNT) is also a carbonaceous material consisting of rolled up graphene sheets. The presence of CNT in the polymer could enhance the concentration of polycyclic aromatic hydrocarbon (PAH) adsorbed to the particles emitted from the combustion of reinforced polyurethane (PU) and polycarbonate (PC) (Singh et al., 2017). Watson-Wright et al. showed that the particulate emissions from PU-CNT (delivered doses of 0.06, 0.6 and 6 μg/cm^2) caused an increase in reactive oxygen species (ROS) formation and a decrease in mitochondrial membrane potential compared to the emissions from PU in primary small airway epithelial cells. The emissions from the combustion of the pure polymers (polypropylene (PP) and PC) and the polymer composites (PP-CNT and PC-CNT) induced ROS formation, but they did not observe any difference in the adverse outcomes between the pure polymers and the composites (Watson-Wright et al., 2017). Coyle and co-workers demonstrated that PC-CNT showed approximately 2-fold more cytotoxicity than PC in human bronchial epithelial cells (BEAS-2B). Moreover, the cells exposed to 1.2 μg/cm^2 of the combustion emissions of PC-CNT showed a significant increase in the intracellular ROS formation and DNA damage at 48 h, whereas the cells exposed to the combustion emissions of PC did not show any cytotoxicity. On the other hand, emission from PU and PU-CNT was not cytotoxic to BEAS-2B (Coyle et al., 2020). Hufnagel et al. investigated the *in vitro* toxicity of combusted CNT, pure polyethylene (PE), and PE-CNT on A549 cells *via* air-liquid interface (ALI) exposure. They found that the combusted PE and PE-CNT induced cytotoxicity at 24 h, while the combusted CNT did not (Hufnagel et al., 2021). Despite discrepancies in the literature, it is clear that the type of polymer matrix, the physicochemical properties and loading of nanofiller could affect the particles and gases released from the combustion of the nanomaterial-embedded polymer composites and subsequently their potential hazard (*Health hazards of composites in fire,* 2006; Motzkus et al., 2011; Singh et al., 2017), which has to be assessed case-by-case.

To our best knowledge, there is currently no information available on the airborne emissions from the combustion of GNP-reinforced polymer and potential human health risks upon inhalation. Therefore, in this study, we have established a new platform to investigate the characteristics and potential hazard of the emissions from the combustion of GNP-reinforced polymer. Our previous study (Netkueakul et al., 2020b) has shown that GNP with the lateral dimension of 25 μm could induce oxidative stress and reduce the cell viability of human macrophages (THP-1); therefore, we used this GNP as the filler in epoxy composite for this study. The epoxy and GNP-reinforced epoxy served as a model system of GNP-reinforced polymer, on which we had full knowledge of the fabrication process and characterization. The platform combines a cone calorimeter (a standard fire analytical instrument), two real-time particle size distribution measurement instruments (an aerodynamic particle sizer and a fast mobility analyzer), a particle collection system for off-line analysis, and an on-line cell exposure system for *in vitro* cytotoxicity assessment. As a biological model for the lung epithelium, we examined the biological consequences at two time points (24 h and 96 h) of the airborne emissions on differentiated A549 monolayer cultures exposed directly to the emissions at ALI conditions, which more realistically resemble the conditions in the lung. The deposited doses of the emissions were based on the realistic graphene-related materials (GRM) exposure concentrations (Drasler et al., 2018). This study provides new insights on the characteristics and toxicity of emissions from the combustion of GNP-polymer composites, which is imperative for the safe and sustainable design and the use of these promising materials.

2. Materials and methods

2.1. Epoxy and epoxy-graphene nanoplatelet composite

Diglycidyl ether of bisphenol A, DGEBA (Araldite GY 250, Huntsman, USA) and an aliphatic polyetheramine (Jeffamine D-230, Huntsman, USA) were used as epoxy and hardener, respectively. GNP (XG Science, Lansing, MI, USA) had lateral dimension of 25 μm according to the manufacturer and the detailed characterization can be found elsewhere (Netkueakul et al., 2020b). EP and EP-GNP composites were fabricated as described elsewhere (Netkueakul et al., 2020a).

2.2. Combustion experiment and exposure system

The sample (10 cm width × 10 cm length and 4 mm thickness) was combusted using an FTT cone calorimeter (Fire Testing Technology, West Sussex, United Kingdom) with the heat flux of 50 kW/m^2 (~750 °C). The exhaust pipe of the cone calorimeter was modified for the sampling probe, which was positioned above the flame. The soot

from the combustion was sampled to on-line particle characterization instruments, a filter for particle collection, and a cell exposure chamber as shown in Fig. 1. Two samples were combusted consecutively for each cell exposure experiment to achieve a deposited dose that was comparable to the doses used in other *in vitro* inhalation studies (Chortarea et al., 2017, 2015; Drasler et al., 2018). Three biologically independent experiments were performed for each time point (24 h and 96 h).

The on-line particle size distribution characterization consisted of a fast mobility analyzer (DMS 500, Cambustion, Cambridge, UK) and an aerodynamic particle sizer (APS, Model 3321, TSI, Shoreview, MN, USA). The cell exposure chamber consisted of an inlet on the top where the emissions enter the chamber. The four outlets at the bottom of four walls of the exposure chamber were connected to a filter (AX1720HD, Lydall, Manchester, CT, USA) for particle collection. The flow rate was controlled using a mass flow controller (Aalborg, Orangeburg, NY, USA) and set at 8 L/min. A quartz crystal microbalance (QCM, openQCM wi2, Pompeii, Italy) was placed inside the chamber to monitor the doses of deposited particles. Sauerbrey equation was applied to estimate the mass of the deposited particles based on the frequency change of the quartz crystal (Buttry and Ward, 1992; Xiao et al., 2020). Additionally, Si wafer grids were placed in the well plate to collect the deposited particles for scanning electron microscopy (SEM, Nova NanoSEM 230, FEI Company, Hillsboro, OR, USA) analysis. The number and size of the deposited particles obtained from SEM images in the area of 760 μm^2 were analyzed using ImageJ software.

2.3. Off-line particle characterization

Particle morphology and elemental composition of pristine GNP and soot were analyzed using the SEM equipped with an energy dispersive X-ray spectrometer (SEM-EDX, Nova NanoSEM 230). X-ray diffractometer (X'Pert Pro, Malvern Panalytical, Malvern, UK) was employed to determine the X-ray diffraction patterns of the pristine GNP and soot and residual ash from combustion with the scan range between 5 and 80° and a scan speed of 0.02°/s. Raman spectroscopy mapping measurements were performed on a Senterra Raman spectrometer (Bruker, Billerica, MA, USA). We used an excitation laser with a wavelength of 532 nm and a power of 2 mW and 50× objective lens. Each Raman spectrum was obtained with an integration time of 20 s per point and co-addition of 2 spectra. The particles were scraped out of the filters and analyzed for 16 PAHs (Table S1) using gas chromatography-flame ionization detector (GC-FID). The extraction and analytical methods were compliant with NIOSH 5515 with some modifications. Details can be found in SI.

2.4. Evaluation of biological responses

2.4.1. Cell culture

Human alveolar pulmonary epithelial cell line (A549, American type culture collection CCL-185, Lot number 60120896) was cultivated in complete cell culture medium (Rosewell Park Memorial Institute (RPMI)-1640 medium, Sigma-Aldrich) supplemented with 10% fetal calf serum (Sigma-Aldrich), 1% L-glutamine (Sigma-Aldrich) and 1% penicillin–streptomycin–neomycin (Sigma-Aldrich) in T75 cell culture flasks. Cells were maintained at 37 °C and 5% CO_2 in humidified atmosphere and routinely sub-cultured twice a week. The cells (5×10^5 cells per insert) were seeded on the apical side of microporous culture inserts (PET, pore diameter 3 μm, 113.1 mm^2 growth area, Thincerts™, Greiner Bio-One Vacuette Schweiz GmbH, St. Gallen, Switzerland). The cells were cultivated in submerged condition for 96 h, where 1.5 mL complete cell culture medium was added on the basolateral side and 1 mL on the apical side. After 96 h, the cells were transferred to ALI conditions (by removing the apical medium) and kept for 24 h prior to the exposure. For the exposure, the cells were transferred to the cell exposure chamber of the platform, without gas composition or temperature control, for 15 min (with the lid of the chamber removed) during the burning of the composites and then transferred back to the cell culture incubator. After the exposure, cells were incubated for 24 h or 96 h and then analyzed or stored for further analysis. Positive controls for each assay were applied to the cells (100 μL of the indicated controls on apical side) on the day of an exposure experiment unless stated otherwise. Negative control cultures were the cells exposed to filtered air (8 L/min) for 15 min.

2.4.2. Cell morphology

Confocal laser scanning microscope (CLSM, LSM780, 40× objective lens, Carl Zeiss AG, Switzerland) was employed to investigate cell morphology. The cells were fixed in 4% paraformaldehyde (PFA, in PBS, Sigma Aldrich) and permeabilized with Triton X-100 (0.2% *v*/v in PBS, Sigma Aldrich). Rhodamine phalloidin (Invitrogen; 1:40 in 1% BSA/PBS) was used to stain F-actin and DAPI (4′,6-diamidino-2-phenylindole, Life Technologies, Thermo Fisher Scientific, Switzerland; 1:1000 in 1% BSA/PBS) was used to label the nucleus. After incubation for 2 h without light at room temperature, inserts were washed with PBS, mounted on glass slides using Mowiol (Sigma Aldrich), and stored at 4 °C until the analysis.

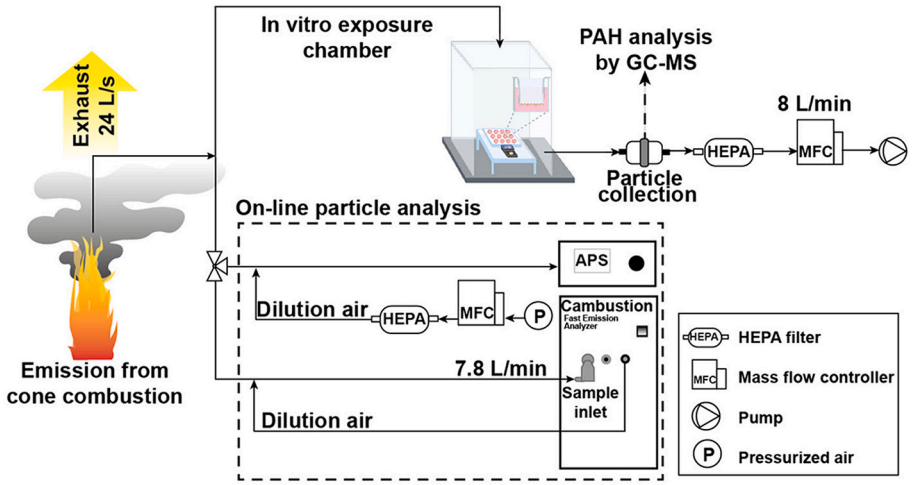

Fig. 1. Scheme of the set-up of the combustion experiment consisting of a cell exposure chamber for *in vitro* toxicity assessment, collection of particles emitted from the combustion for PAH analysis, and on-line aerosol characterization instruments. The drawing of the cell exposure chamber was created using Biorender. GC–MS is gas chromatography–mass spectrometry; MFC is mass flow controller; APS is aerodynamic particle sizer.

2.4.3. Cell viability

Lactate dehydrogenase (LDH) release from cells is an indicator of cell membrane integrity and the quantification of LDH is used to assess cytotoxicity. Cell culture media at basolateral side were collected and analyzed using CytoTox96® Non-Radioactive Cytotoxicity Assay (Promega Corporation, Madison, Wisconsin, USA) following the manufacturer's protocol with some modification. The cells exposed to 0.5% v/v Triton X-100 (Sigma-Aldrich) in PBS for 1 h were used as positive control. 3-(4,5-di- methylthiazol-2-yl)-5-(3-cyrboxymethoxy-phenyl)-2-(4-sulfophenyl)-2H-tetrazolium, inner salt (MTS) assay, an indicator of mitochondrial activity, was performed using the CellTiter96 Aqueous One solution (Promega). Positive control cultures were treated with 10^4 μM $CdSO_4$ (apically). The Mithras2 microplate reader (Berthold Technologies, Germany) was used for colorimetric measurements. The cell viability was reported relative to the negative control (filtered air exposure). Detailed procedures of LDH and MTS assays can be found in SI.

2.4.4. Cytokine profiling

The cellular (pro-) inflammatory responses are associated with the amounts of released cytokines and chemokines in cell culture media. Samples were sent to Eve Technologies (Alberta, Canada) for quantification of 15 crucial (pro-) inflammatory cytokines using multiplex technology (Bioplex, Biorad). The cytokine array included the following inflammatory markers: granulocyte-macrophage colony-stimulating factor (GM-CSF), monocyte chemoattractant protein-1 (MCP-1), tumor necrosis factor alpha (TNF-α), interferon gamma (IFNγ), interleukin 1β (IL-1 β), IL-1ra, IL-5, IL-6, IL-8, IL-12(p70), IL-13, IL-2, IL-4, IL-10, and IL-12(p40). For each repetition, the media in basolateral part from three wells were collected in the same tube. Three repetitions were performed and the samples from each repetition were analyzed in duplicates.

2.4.5. Gene expression analysis

At 24 h and 96 h after exposure to the emissions, membranes containing cells were cut from the inserts and preserved in 500 μL of RNA protection buffer (Qiagen AG, Hombrechtikon, Switzerland) until RNA isolation. RNA was isolated using miRNeasy Mini Kit following the manufacturer's protocol (Qiagen). The real-time reverse transcriptase polymerase chain reaction (RT-PCR) was carried out with a 96-well fast reaction PCR system (C1000 Touch™ Thermal Cycler, Bio-Rad Hercules, CA, USA). The complementary DNA (cDNA) was synthesized using the isolated RNA, iScript reaction mix (Bio-Rad Laboratories, Hercules, CA, USA) and iScript reverse transcriptase (Bio-Rad Laboratories). The reverse transcriptase reactions were performed by combining cDNA and iQ SYBR Green Master mix. The relative expression values of the target mRNA was calculated using the $^{\Delta\Delta}$Ct method (Schmittgen and Livak, 2008) and glyceraldehyde-3-phosphate dehydrogenase (*GAPDH*) was used as a reference gene. Two anti-oxidative stress markers heme oxygenase 1 (*HMOX1*) and superoxide dismutase 2 (*SOD2*) were assessed. Aryl hydrocarbon receptor (AhR) activation was evaluated using cytochrome P450 1A1 (*CYP1A1*) gene. The primer sequences for all tested genes are reported in Table S2 in SI.

2.4.6. Statistical analysis

Data were analyzed in three repetitions and all assays were performed at least in duplicates. All results are presented as mean ± standard error of the mean and p values <0.05 were considered statistically significant. A Turkey post-hoc test was performed using R to compare the means among filtered air control, emissions from EP, and emissions from EP-GNP.

3. Results and discussion

3.1. Combustion characteristics of EP and EP-GNP

In our combustion experiment, we employed the cone calorimeter, a standardized instrument to study the fire behavior of materials according to ISO 5660-1. This allowed us to investigate the effects of nanofillers on the combustion behavior in a controlled manner. To this end, the heat flux of 50 kW/m^2 that yielded a temperature lower than 800 °C was selected, since it represents the fully developed fire (International Organization for Standardization, 1989) and a temperature higher than 800 °C might destroy the GNP (Hahn, 2005). It is important to note that the combustion temperature used in this study might not represent the incineration process, which uses higher temperature ranging from 850 °C to over 1100 °C. Nevertheless, our study provides information related to the effects of the incorporation of GNP to the polymer on the emissions from combustion in a controlled environment, which might be relevant to combustion conditions in certain accidental fires. Some observed effects such as delayed ignition, reduced HRR, reduced pHRR, or decreased total heat release have been commonly reported in previous studies (Laachachi et al., 2015; Liu et al., 2016; Yu et al., 2015), which covered different heat fluxes and combustion temperatures; however, we did not focus on temperature effects on the emissions. There is still a need to further investigate the effects of the heat flux and combustion temperature on the combustion emissions in the future.

The change in combustion profile could affect the physicochemical properties of the emissions and subsequently their potential hazard. The cone calorimetry revealed the fire characteristics of EP and EP-GNP during the combustion and important parameters are summarized in Table S3. The combustion of each sample lasted 5 to 7 min. Plots of the heat release rate, which represent the combustion profile of the samples, showed peaks at around 130–140 s (Fig. S1). GNP slightly delayed the time to ignition of epoxy composite, as shown in Table S3, due to the good thermal diffusivity of GNP, which helped to diffuse the heat from material's surface to the bulk (Laachachi et al., 2015). The effect of adding GNP was a slight reduction in the peak heat release rate (pHRR) and a small enhancement in CO production, which led to an increase in the CO/CO_2 ratio. Theoretically, as a flame retardant, GNP should decrease the heat release rate (HRR) and pHRR. Although we observed a slight reduction in the pHRR for EP-GNP, EP-GNP showed higher HRR at 50–150 s as compared to EP. We hypothesized that the presence of GNP could lead to the competition between the good thermal conductivity and the barrier formation ability of the GNP in the composite (Liu et al., 2014). Studies showed an increase in thermal conductivity of the epoxy composite when the GNP loading increased (Chatterjee et al., 2012; Wang et al., 2009). The higher thermal conductivity of GNP than the epoxy resin might have contributed to the higher HRR observed in EP-GNP. When the combustion progresses, the viscosity of the polymer matrix decreases as the temperature rises, which can lead to the migration of the GNP to the top surface of the composite due to the relatively low density of GNP. The GNP could form a network on the surface, which might act as a physical barrier, shielding the heat released and delaying the release of the combustible gases to the flame zone, thus could delay the combustion process. Liu *et al* also observed an increase in HRR and pHRR as the GNP loading increased (Liu et al., 2014). Therefore, we presumed that the loading amount of GNP in our study might not be sufficient for the barrier effect to become dominant. Literatures reported the reduction of HRR at higher GNP loading as follows: a 47% reduction of pHRR at 3 wt% GNP loading in epoxy composite (Zhang et al., 2018) and a 72% reduction in pHRR at 5 wt% GNP loading in PP composite (Dittrich et al., 2013). Higher CO/CO_2 ratio indicates that the combustion is more incomplete. Since we observed differences in the types and concentrations of PAH between the particulate emissions from EP and those from EP-GNP, we speculated that an increase in the degree of incomplete combustion in the presence of GNP could influence the chemical composition of the emission.

3.2. Particle characterization

3.2.1. Particle size distribution

The presence of GNP affected neither the particle number nor the

particle size of the emissions. Total concentrations of the emissions from burning EP and EP-GNP measured by DMS500 (Fig. S2) had the peaks in the range of 10^9 particles/cm^3. Fig. 2a showed that the particle size distributions had the peak concentrations between 100 s and 200 s of the burning time, which matched well with the time window of peak heat release rate in cone calorimetry. Since the combustion was a dynamic process, different size distributions were observed over the burning period. However, similar characteristics of particle size distributions were detected from the combustion of EP and EP-GNP. Before the peak emissions (during 0–100 s), the average particle size distribution revealed two particle modal sizes at around 20 nm (the dominant mode) and at around 200 nm. At the peak emissions (101–250 s), the dominant particle mode was at approximately 15 nm and another mode was at around 150 nm, which was challenging to detect due to its relatively low concentration compared to the first mode. After the peak emissions (from 251 s), the particle modes were at 15 nm and 200–300 nm. Particles in micrometer range analyzed by APS showed that particle modes were between 1 and 2 μm (Fig. 2b). The results from DMS500 and APS suggested that the sizes of particulate emissions from burning EP and EP-GNP were smaller than 4 μm, which fell into the respirable fraction in the alveolar region of the lung (Hofmann, 2011).

3.2.1.1. Raman spectroscopy mapping and XRD of the particulate emissions. Raman spectroscopy is a useful tool to study graphitic materials because they show distinctive patterns consisting of D band (1355 cm^{-1}), G band (1581 cm^{-1}) and 2D band (~2700 cm^{-1}). Details can be found in SI. The degree of defects on the graphitic sheets is associated with the shift of the G peak position and the intensity ratio of D band to G band (I(D)/I(G)) (Ferrari and Robertson, 2000). D, G and 2D band positions and I(D)/I(G) were obtained from Raman spectroscopy mapping of pristine GNP, soot and residues from the combustion of EP and EP-GNP (Fig. S3a, Fig. S4, and Table S4). I(D)/I(G) of the soot and residues of EP and EP-GNP was higher than the pristine GNP. The residues of EP and soot of both EP and EP-GNP showed a broad shape of the 2D band, whereas the residues of EP-GNP showed a broad 2D band ranging from 2300 to 3300 cm^{-1} and a relatively sharp peak around 2703 cm^{-1}. The 2D band of graphene sheet usually appears as a sharp peak and becomes broader with increasing disorder (Escribano et al., 2001). The shape of the 2D band suggested that the residues from EP-GNP contained amorphous carbon and ordered structure material, which could be an indication of GNP. The 2D band of the EP residues and soot of EP and EP-GNP showed only a broad band indicating the presence of only amorphous carbon (Escribano et al., 2001).

XRD patterns of soot and residues of EP and EP-GNP were compared with that of pristine GNP (Fig. S3b). The XRD pattern of GNP had a peak at a 2θ of 26.9°, corresponding to the 002 crystal plane of the ordered hexagonal graphite with an interlayer spacing of 3.33 Å. The residues from EP-GNP showed two peaks at 002 position including a peak at 2θ of 26.9°, an indication of ordered structure carbon, and a broad peak with 2θ ranging from 15° to 30°, an indication of amorphous carbon. The residues of EP and soot of EP and EP-GNP only showed a broad peak at 002 position suggesting the absence of the ordered structure carbon (no GNP). Both Raman and XRD results indicated the presence of GNP in the residual ash, not in the aerosol, which could be due to the ability of GNP to form a network-structured layer during the combustion (Dittrich et al., 2013; Liu et al., 2014; Netkueakul et al., 2020a; Zhang et al., 2018) that kept GNP in the residues. Kotsilkov and co-workers also found the release of GNP in the residual ash from burning a PLA-GNP film at 850 °C, but there was no information about the release in an airborne form (Kotsilkov et al., 2018).

3.2.2. Organic compounds analysis

Bar charts in Fig. 3 display the concentrations of PAHs found in particulate emissions and the corresponding equivalent benzo(*a*)pyrene (BaP) concentrations of PAHs. The emission from EP contained more PAH species and higher PAH concentrations than the emission from EP-GNP. Total concentration of 16 PAHs was 35,503 mg PAH/kg of soot for EP emission and 2800 mg PAH/kg of soot for EP-GNP emission, respectively. Pyrene, fluoranthene and phenanthrene have the highest concentrations among the PAHs analyzed in the particulate emission from EP, whereas PAHs with the highest concentrations found in the particulate emission from EP-GNP were pyrene, fluoranthene and benzo(*a*)pyrene.

In terms of toxic potential, emissions from EP showed higher

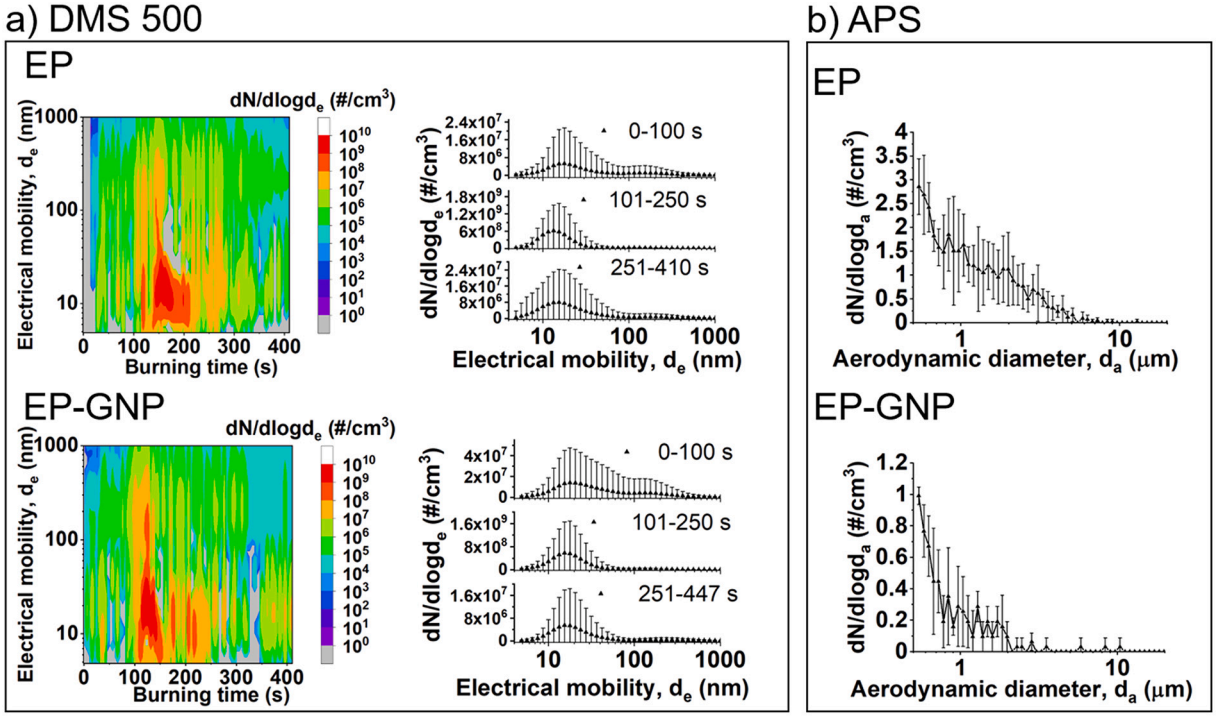

Fig. 2. Particle size distributions of airborne emissions from the combustion of EP and EP-GNP measured by a) DMS500 and b) APS.

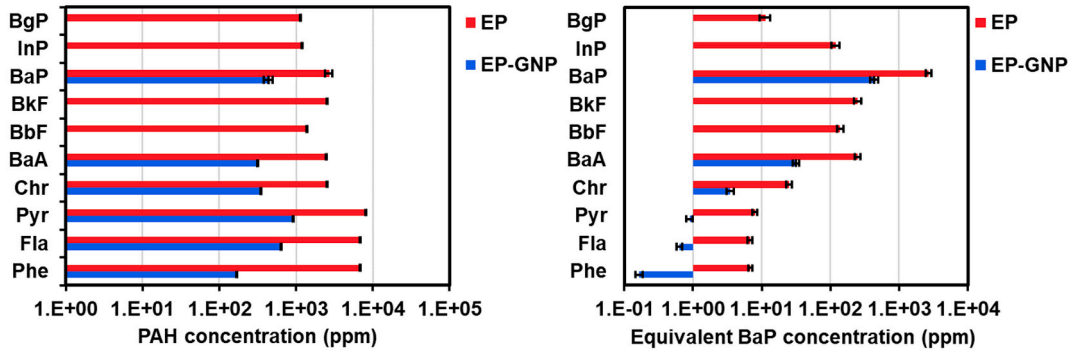

Fig. 3. a) Comparison between PAH concentrations (mg PAH per kg of particles (ppm)) emitted from the combustion of EP and EP-GNP and b) the corresponding toxic potential of each PAH presented as the equivalent benzo(*a*)pyrene concentration (Nisbet and LaGoy, 1992) (mg PAH per kg of particles (ppm)). Bar charts show average values and error bars indicate standard deviations obtained from two analyses of one collected sample. The analyzed PAHs included naphthalene (Nap), acenaphthylene (Acy), acenaphthene (Ace), fluorene (Flu), phenanthrene (Phe), anthracene (ant), fluoranthene (Fla), pyrene (Pyr), chrysene (Chr), benzo(*a*) anthracene (BaA), benzo(*b*)fluoranthene (BbF), benzo(*k*)fluoranthene (BkF), benzo(*a*)pyrene (BaP), indeno(1,2,3-c,d)pyrene (InP), dibenzo(*a*,*h*)anthracene (DaA), and benzo(*g*,*h*,*i*)perylene (BgP).

equivalent BaP concentrations than those from EP-GNP. The levels of total equivalent BaP concentration of the analyzed PAHs were 3515 mg PAH/kg of soot and 475 mg PAH/kg of soot for EP and EP-GNP emissions, respectively. BaP contributed to the highest equivalent BaP concentration for both emissions and other PAH species were at least one order of magnitude lower in the equivalent BaP concentration as shown in Fig. 3b.

Graphene platelets are known for their unique electron accepting and π-π interaction ability, which enable graphene platelets to be an exceptional adsorbent towards organic molecules such as PAHs (Wang et al., 2014; Zhang and Xi, 2011). Our XRD and Raman results demonstrated the presence of GNP in the residues of EP-GNP after combustion, indicating that GNP was not completely decomposed by the combustion process. We hypothesized that the presence of GNP could reduce the concentrations of PAH species formed during the combustion *via* adsorption onto GNP surface, probably due to high adsorption affinity of PAH to the surface of GNP. Vejerano *et al* also reported that the presence of C_{60}-fullerene at 10 wt% could reduce the concentration of PAHs in the emissions during the combustion of poly(vinyl chloride) (PVC) as compared to those of the bulk PVC (Vejerano et al., 2013). However, the enhancement of PAH concentrations has been reported when the concentration of injected C_{60}-fullerene was 0.1 wt% or during the combustion of other materials such as paper and polyethylene (Vejerano et al., 2013). Moreover, Singh and co-workers reported the effect of CNT on the enhancement of PAH profile of the particles released from thermal decomposition of thermoplastics (Singh et al., 2017). They showed that the degree of increase in PAH concentrations varied depending, not only on the type of nanofiller, but also on the type of matrix. Although GNP, C_{60}-fullerene, and CNT are carbonaceous material, they have distinct morphologies, which could play a crucial role in PAH adsorption (Ersan et al., 2017).

3.3. Evaluation of biological responses

We assessed the biological response of alveolar epithelial cells at 24 and 96 h after exposure to the emissions, which allowed us to study acute and chronic cellular effects. The human alveolar epithelial Type II cells (A549) were used in our study because they are polarized and produce surfactant similar to *in vivo* conditions and they have been employed in many ALI studies with nanomaterials (Kooter et al., 2016; Leibrock et al., 2020). Moreover, cells were maintained at ALI conditions, which more realistically resembled the *in vivo* situation.

For toxicity evaluation, it is crucial to exclude interferences from particles with the assays (Kroll et al., 2012). For our studies, we mostly used basolateral supernatants, which should be largely free of particles, since translocation of nanoparticles across biological barriers is often low (few percentages of the applied dose) (Doryab et al., 2021) {Doryab, 2021 #314}and samples were centrifuged before further analysis to remove translocated particles. Moreover, we have shown in a previous study that GNPs did not interfere with LDH and ELISA assays at concentrations up to 15 μg/mL (Drasler et al., 2018). For MTS assay, we showed in another study that GNPs did not cause any interference responses with the MTS assay even at very high concentrations up to 40 μg/mL (Netkueakul et al., 2020b).

3.3.1. Deposited dose determination

The QCM measurements of the filtered air showed no frequency change during the exposure period over 15 min (Fig. S6), indicating that the deposited particles during the filtered air exposure were below the detection limit of QCM (1 ng/cm^2 according to manufacturer). The QCM results and the SEM images showed a reproducible and controlled deposition of combustion particles. Results from QCM (Fig. S7) revealed that the average deposited doses of the emissions from EP and EP-GNP were in the similar range, specifically 0.27 ± 0.08 μg/cm^2 for EP and 0.29 ± 0.08 μg/cm^2 for EP-GNP. Fig. S8 showed the SEM images and the corresponding particle size distributions of the uniformly deposited particles in the well-plate, which were comparable between EP and EP-GNP. Only one deposited dose was investigated in this study because our exposure system was not equipped with the controlled humidified atmosphere and CO_2 concentration, which may cause negative impacts to the cells when the exposure period was prolonged to enhance the particle deposition. In addition, the deposited doses (mass per surface area) in this study were in the same range as those reported in other *in vitro* toxicity studies that performed an air-liquid interface aerosol exposure to carbonaceous materials (CNT, GNP, graphene oxide) or emissions from the combustion of polymer nanocomposites (TiO_2, CuO, or CNT nanofillers) (Chortarea et al., 2017, 2015; Drasler et al., 2018; Hufnagel et al., 2021).

3.3.2. Cell morphology and viability

Immunocytochemical staining revealed that the cells treated with filtered air, which was used as the negative control, did not show any significant differences in cell morphology and monolayer integrity compared to the untreated cells (Fig. S9). There were no apparent changes in cell morphology after cell exposure to emissions from EP and EP-GNP as compared to filtered air exposure even at 96 h post-exposure time (Fig. 4a). Cell viability was evaluated by the release of LDH (membrane integrity) and MTS assay (mitochondrial activity) (Fig. 4b–c). Emissions from the combustion of EP did not affect membrane integrity or mitochondrial activity of the cells up to 96 h post-

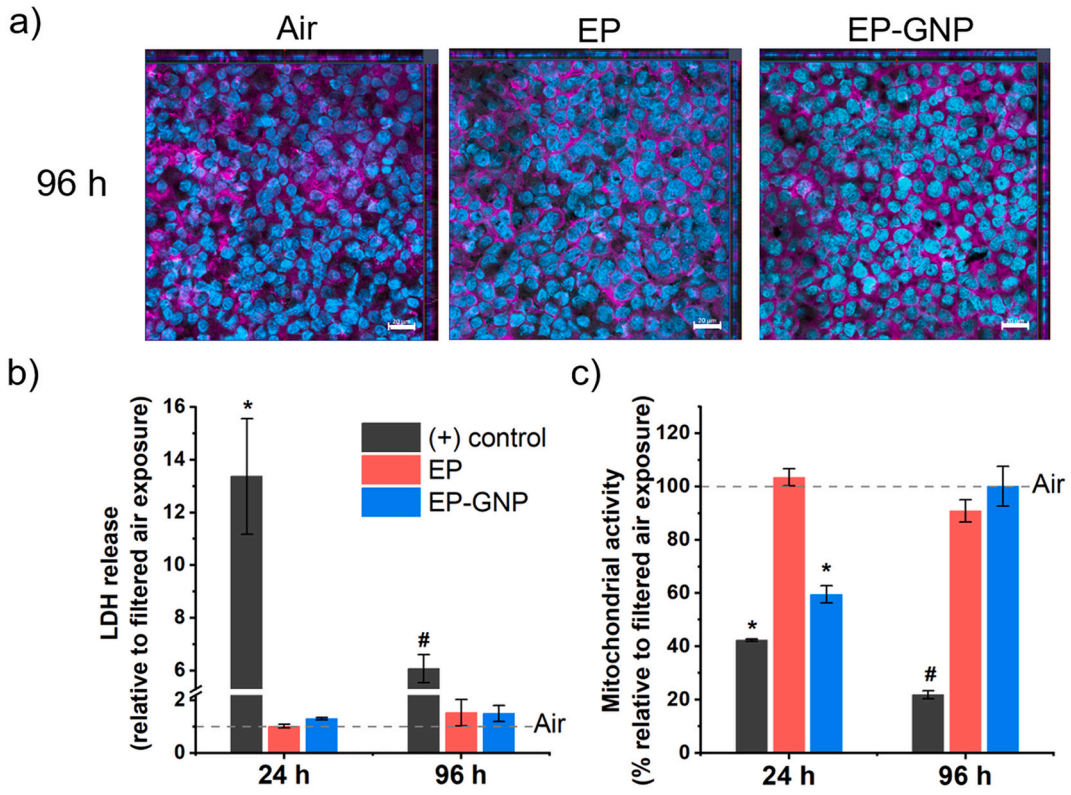

Fig. 4. a) Cell morphology at 96 h after exposure to filtered air and emissions from combustion of EP and EP-GNP analyzed using confocal laser scanning microscopy. Blue = DAPI; magenta = Rhodamine phalloidin. The scale bar is 20 μm. Cell viability determined by measuring b) the release of lactate dehydrogenase (LDH assay) and c) mitochondrial activity (MTS assay). Triton X-100 (0.5% *v*/v) and $CdSO_4$ (10^4 μM) were used as (+) controls for LDH and MTS assays, respectively. Bar chart displays average values of three experiments and error bars are standard error of mean. Symbol * and # indicate statistically significantly different from the filtered air exposure ($p < 0.05$). (For interpretation of the references to colour in this figure legend, the reader is referred to the web version of this article.)

exposure. For emissions from EP-GNP combustion, a transient decrease in mitochondrial activity (significant at 24 h, $p < 0.05$; recovered to negative control levels at 96 h) was observed, but this did not lead to cell death as evidenced by the lack of LDH release at both investigated time points. It is noteworthy that LDH degrades in cell media across time with a half-life of 9 h (Welch et al., 2021). It is possible that some fractions of the cells were killed and released LDH, but the LDH then degraded up to the 96-h time point, showing a lack of toxicity. However, there was no effects in MTS or immunocytochemistry staining that would indicate any early cell death response.

3.3.3. *Cytokine profiling*

To estimate potential (pro-) inflammatory responses of the airborne emissions, we performed a cytokine profiling of 15 cytokines and chemokines. The relative concentrations of 10 cytokines, including TNF-a, MCP-1, IL-8, IL-6, IL-5, IL-1Ra, IL-12p70, IL-10, IFNγ and GM-CSF, released into cell culture media compared to filtered air control were displayed in Fig. S10. IL-13, IL-2, IL-4, IL-10, and IL-12(p40) were also included in the Bioplex panel; however, their release levels were below the limit of detection for the experimental set-up. After exposure to EP and EP-GNP emissions, all the cytokines, except MCP-1 and GM-CSF, were at similar levels as the cells exposed to filtered air. Both MCP-1

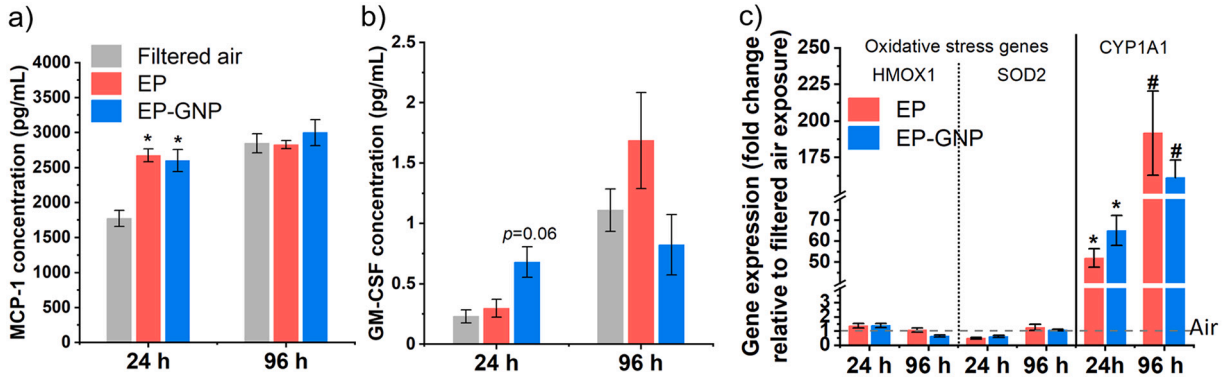

Fig. 5. Release of two cytokines/chemokines including a) monocyte chemoattractant protein-1 (MCP-1) and b) granulocyte-macrophage colony-stimulating factor (GM-CSF). c) Expression of two oxidative stress genes (*HMOX1* and *SOD2*) and aryl carbon receptor gene *CYP1A1* in comparison to filtered air exposure (negative control). Bar charts present average values from three experiments ± standard error of mean. Symbol * and # indicate statistically significantly different from negative control ($p < 0.05$).

and GM-CSF are associated with (pro-) inflammatory responses and GM-CSF also contributes to the development of autoimmune and inflammatory diseases (Shiomi and Usui, 2015). We found a significant increase in the secreted MCP-1 in cell culture media at 24 h after exposure to emissions from both EP and EP-GNP compared to filtered air exposure, whereas at 96 h the MCP-1 levels in these samples were comparable to filtered air exposure (Fig. 5a). EP-GNP further induced a noticeably higher level of the growth factor of GM-CSF than filtered air exposure ($p = 0.064$) at 24 h, while EP also induced a slightly higher GM-CSF level at 96 h compared to EP-GNP and filtered air exposure; nevertheless, these increases were not statistically significant (Fig. 5b). Since the expressions of the other key cytokines/chemokines in the array were not affected, the increased MCP-1 indicated only a limited (pro-) inflammatory response. The release of MCP-1 and GM-CSF is cellular protective mechanisms in response to oxidative stress, cytokines, or growth factors *via* recruiting monocytes (Deshmane et al., 2009) and activating granulocytes and macrophages, respectively (Shiomi and Usui, 2015). The release of MCP-1 and GM-CSF was previously reported when cells were treated with particles from diesel exhaust or aircraft turbine engine exhaust (Baulig et al., 2003; Jonsdottir et al., 2019; Ohtoshi et al., 1998).

3.3.4. Gene expression analysis

No significant alteration in the expression levels of two oxidative stress-related genes, *HMOX1* and *SOD2*, was detected from exposure to either EP or EP-GNP emissions at 24 h and 96 h time point (Fig. 5c). It is well known that oxidative stress is closely related to inflammatory responses (Reuter et al., 2010). Although EP and EP-GNP could induce the release of (pro-) inflammatory mediator MCP-1, we did not observe any significant deregulation on the expression levels of the oxidative stress related genes *HMOX1* and *SOD2*.

The expression level of *CYP1A1* gene was upregulated by 50-fold at 24 h after exposure to emissions from the combustion of both EP and EP-GNP and further increased by 150-fold at 96 h time-point (Fig. 5c). This significant increase in *CYP1A1* expression suggested a strong cellular response to PAHs, which is responsible for metabolism of PAHs *via* the aryl hydrocarbon receptor (Shimada and Fujii-Kuriyama, 2004). Although particulate emissions from EP had higher PAH concentrations than those from EP-GNP, there was no significant difference in the expression level of *CYP1A1* gene between both emissions. Previous studies showed that the presence of PAHs induced an increase in the expression level of *CYP1A1* in A549 cells (Castorena-Torres et al., 2008) in a dose-dependent manner (Genies et al., 2013). On the other hand, some PAHs could inhibit CYP1 family enzymes *i.e.* CYP 1A1, 1A2 and 1B1 and consequently affect the metabolisms of xenobiotics catalyzed by these enzymes (Shimada and Guengerich, 2006). Overall, despite some differences in the absolute PAH levels, the response in *CYP1A1* activation was rather similar for EP and EP-GNP emissions. However, more genes associated with aryl hydrocarbon receptor should be analyzed to better understand the possible impact of PAHs.

Despite a decrease in mitochondrial activity at 24 h after exposure, EP and EP-GNP did not show any significant difference in other cytotoxicity markers. Since we detected GNP only in residual ash, GNP (if any) was not likely to directly contribute to the biological effects of the aerosol emissions found in this study. Apart from PAHs adsorbed to particles, PAHs and other toxic compounds in the gas phase such as NO_x and CO could have formed during the combustion of epoxy composites and caused adverse cellular effects.

The contribution of the soot fraction to the difference in biological effects caused by the emissions from the combustion of EP-GNP compared to those of EP was unlikely since the deposited doses in both cases were not statistically different. Moreover, the particle size distributions of the emissions from EP and EP-GNP measured by APS and DMS500 were also in a similar range. Dilger and co-workers studied the contributions of soot, metals, and PAHs, which were the components of the wood smoke particles, to the biological effects of A549 under submerged exposure conditions (Dilger et al., 2016). The soot and PAHs contributions were mimicked using carbon black and BaP, respectively. They found that PAHs adsorbed to wood smoke particles did induce PAH metabolism by *CYP1A1* to a higher extent than the pure BaP. Mitochondrial activity of A549 cells after exposure to carbon black up to 100 μg/mL (31.25 μg/cm^2) was not decreased, but increased, and LDH release was not affected. Carbon black, representing soot fraction, with the delivered doses of 50 and 100 μg/mL and metals could induce ROS formation (Dilger et al., 2016). In our study, the deposited doses (0.27–0.29 μg/cm^2) were much lower and did not result in an oxidative stress response (as demonstrated by the *HMOX1* and *SOD2* expression). Hufnagel et al. also analyzed whether particles and/or gases contributed to the toxic effects of the emissions from the combustion of nanomaterial-embedded polymer by comparing the whole emissions to the particle-filtered emissions (Hufnagel et al., 2021). They did not observe any difference in the biological effects on A549 cells after exposure to the whole emissions or the gaseous phase, concluding that the toxic effects were entirely due to the gaseous phase in the emissions such as CO and volatile and semi-volatile organic compounds (Hufnagel et al., 2021). In summary, the reason for the transient reduction in mitochondrial activity caused by EP-GNP but not EP emissions remains to be identified.

4. Conclusions

In the present study, we have established and utilized a platform to investigate the effects of GNP nanofiller in epoxy composite on the aerosol released from the combustion in terms of their particle size and concentration, PAH concentration, and biological effects on lung cells. The concentrations of the released aerosols were in the range of 10^9 particles/cm^3 and their sizes ranged from tens of nanometers to a few micrometers, which is in the respirable size range. The presence of GNP did not alter the particle size distributions of the emissions formed during the combustion of the epoxy. Raman spectroscopy and XRD analysis of the particulates formed in the combustion process confirmed the absence of GNP in the airborne fraction emitted from the combustion of EP-GNP, while GNP were found in the residual ash. Despite its absence in the airborne fraction, the presence of GNP in EP composite could reduce the PAH concentration on the particles released from the combustion. After exposure to EP and EP-GNP combustion emissions, we did not observe any change in cell morphology, any severe cytotoxicity, release of (pro-) inflammatory factors, nor a change in the expression levels of oxidative stress markers, *HMOX1* and *SOD2*, indicating the absence of an acute cytotoxic effect. Emissions from EP and EP-GNP strongly affected the PAH metabolism in the cells (upregulation of *CYP1A1*). Our results confirm the potential health risks of the aerosol emissions from epoxy composites at their end-of-life *via* a combustion process, at the same time highlight that incorporation of GNP is not inducing any novel or additive adverse effects on alveolar epithelial cells within 96 h of culture after exposure. However, longer exposure time and long-term effects of these emissions should be further investigated.

Author contributions

W.N. fabricated epoxy composites and characterized the physicochemical properties of GNP and emissions from the combustion. W.N., S·C., and J.W. designed the combustion exposure experiment. W.N. and S.C. performed *in vitro* toxicity assessments. W.N., S.C., and K.K. analyzed the toxicity data. W.N., L.H., and K.K. analyzed PAH data. W.N. and G.Q. performed Raman spectroscopy mapping and analyzed the Raman data. W.N., S.C., Y.H., and M.J. performed the combustion and exposure experiments. Y. H. maintained the cell culture. M.J. calibrated the cone calorimeter. S.G. supported with the cone calorimeter and fire behavior analysis. S.C designed and supervised the *in vitro* experiments. T.B.T. and P.W. supervised and supported with the *in vitro* toxicity assessment. P. W. and J.W. initiated the project, conceived the study,

and supervised the study. W.N. wrote the manuscript. All of the authors have discussed the results and have given approval to the final version of the manuscript.

CRediT authorship contribution statement

Woranan Netkueakul: Methodology, Investigation, Writing – original draft, Visualization. **Savvina Chortarea:** Methodology, Validation, Investigation, Writing – review & editing. **Kornphimol Kulthong:** Validation, Investigation, Writing – review & editing. **Hao Li:** Validation, Investigation. **Guangyu Qiu:** Validation, Investigation. **Milijana Jovic:** Validation, Formal analysis. **Sabyasachi Gaan:** Resources, Writing – review & editing. **Yvette Hannig:** Formal analysis, Investigation. **Tina Buerki-Thurnherr:** Validation, Writing – review & editing, Supervision. **Peter Wick:** Conceptualization, Writing – review & editing, Supervision. **Jing Wang:** Conceptualization, Methodology, Writing – review & editing, Supervision.

Declaration of Competing Interest

There are no conflicts of interest to declare.

Data availability

No data was used for the research described in the article.

Acknowledgement

The research leading to these results has received funding from the European Union (EU) Horizon 2020 Framework Graphene Flagship project GrapheneCore2 and GrapheneCore3 (grant agreement n°785219, 881603), the NanoScreen materials challenge co-sponsored by the Competence Centre for Materials Science and Technology (CCMX) as well as Swiss National Science Foundation (grant number 310030_169207).

Appendix A. Supplementary data

Supplementary data to this article can be found online at https://doi.org/10.1016/j.impact.2022.100414.

References

Baulig, A., Sourdeval, M., Meyer, M., Marano, F., Baeza-Squiban, A., 2003. Biological effects of atmospheric particles on human bronchial epithelial cells. Comparison with diesel exhaust particles. Toxicol. in Vitro 17, 567–573. https://doi.org/10.1016/S0887-2333(03)00115-2.

Buttry, D.A., Ward, M.D., 1992. Measurement of interfacial processes at electrode surfaces with the electrochemical quartz crystal microbalance. Chem. Rev. 92, 1355–1379. https://doi.org/10.1021/cr00014a006.

Castorena-Torres, F., de León, M.B., Cisneros, B., Zapata-Pérez, O., Salinas, J.E., Albores, A., 2008. Changes in gene expression induced by polycyclic aromatic hydrocarbons in the human cell lines HepG2 and A549. Toxicol. in Vitro 22, 411–421. https://doi.org/10.1016/j.tiv.2007.10.009.

Chandrasekaran, S., Seidel, C., Schulte, K., 2013. Preparation and characterization of graphite nano-platelet (GNP)/epoxy nano-composite: mechanical, electrical and thermal properties. Eur. Polym. J. 49, 3878–3888. https://doi.org/10.1016/j.eurpolymj.2013.10.008.

Chatterjee, S., Nafezarefi, F., Tai, N.H., Schlagenhauf, L., Nesch, F.A., Chu, B.T.T., 2012. Size and synergy effects of nanofiller hybrids including graphene nanoplatelets and carbon nanotubes in mechanical properties of epoxy composites. Carbon N. Y. 50, 5380–5386. https://doi.org/10.1016/j.carbon.2012.07.021.

Chortarea, S., Clift, M.J.D., Vanhecke, D., Endes, C., Wick, P., Petri-Fink, A., Rothen-Rutishauser, B., 2015. Repeated exposure to carbon nanotube-based aerosols does not affect the functional properties of a 3D human epithelial airway model. Nanotoxicology 9, 983–993. https://doi.org/10.3109/17435390.2014.993344.

Chortarea, S., Barosova, H., Clift, M.J.D., Wick, P., Petri-Fink, A., Rothen-Rutishauser, B., 2017. Human asthmatic bronchial cells are more susceptible to subchronic repeated exposures of aerosolized carbon nanotubes at occupationally relevant doses than healthy cells. ACS Nano 11, 7615–7625. https://doi.org/10.1021/acsnano.7b01992.

Coyle, J.P., Derk, R.C., Kornberg, T.G., Singh, D., Jensen, J., Friend, S., Mercer, R., Stueckle, T.A., Demokritou, P., Rojanasakul, Y., Rojanasakul, L.W., 2020. Carbon nanotube filler enhances incinerated thermoplastics-induced cytotoxicity and metabolic disruption in vitro. Part. Fibre Toxicol. 17, 40. https://doi.org/10.1186/s12989-020-00371-1.

Dao, D.Q., Rogaume, T., Luche, J., Richard, F., Bustamante Valencia, L., Ruban, S., 2014. Thermal degradation of epoxy resin/carbon fiber composites: influence of carbon fiber fraction on the fire reaction properties and on the gaseous species release. Fire Mater. 40, n/a–n/a. https://doi.org/10.1002/fam.2265.

Deshmane, S.L., Kremlev, S., Amini, S., Sawaya, B.E., 2009. Monocyte chemoattractant Protein-1 (MCP-1): an overview. J. Interf. Cytokine Res. 29, 313–326. https://doi.org/10.1089/jir.2008.0027.

Dilger, M., Orasche, J., Zimmermann, R., Paur, H.-R., Diabaté, S., Weiss, C., 2016. Toxicity of wood smoke particles in human A549 lung epithelial cells: the role of PAHs, soot and zinc. Arch. Toxicol. 90, 3029–3044. https://doi.org/10.1007/s00204-016-1659-1.

Dittrich, B., Wartig, K.-A., Hofmann, D., Mülhaupt, R., Schartel, B., 2013. Flame retardancy through carbon nanomaterials: carbon black, multiwall nanotubes, expanded graphite, multi-layer graphene and graphene in polypropylene. Polym. Degrad. Stab. 98, 1495–1505. https://doi.org/10.1016/j.polymdegradstab.2013.04.009.

Doryab, A., Taskin, M.B., Stahlhut, P., Schröppel, A., Orak, S., Voss, C., Ahluwalia, A., Rehberg, M., Hilgendorff, A., Stöger, T., Groll, J., Schmid, O., 2021. A bioinspired in vitro lung model to study particokinetics of nano−/microparticles under cyclic stretch and air-liquid Interface conditions. Front. Bioeng. Biotechnol. 9 https://doi.org/10.3389/fbioe.2021.616830.

Drasler, B., Kucki, M., Delhaes, F., Buerki-Thurnherr, T., Vanhecke, D., Korejwo, D., Chortarea, S., Barosova, H., Hirsch, C., Petri-Fink, A., Rothen-Rutishauser, B., Wick, P., 2018. Single exposure to aerosolized graphene oxide and graphene nanoplatelets did not initiate an acute biological response in a 3D human lung model. Carbon N. Y. 137, 125–135. https://doi.org/10.1016/j.carbon.2018.05.012.

Ermakov, V.A., Alaferdov, A.V., Vaz, A.R., Perim, E., Autreto, P.A.S., Paupitz, R., Galvao, D.S., Moshkalev, S.A., 2015. Burning graphene layer-by-layer. Sci. Rep. 5, 11546. https://doi.org/10.1038/srep11546.

Ersan, G., Apul, O.G., Perreault, F., Karanfil, T., 2017. Adsorption of organic contaminants by graphene nanosheets: a review. Water Res. https://doi.org/10.1016/j.watres.2017.08.010.

Escribano, R., Sloan, J.J., Siddique, N., Sze, N., Dudev, T., 2001. Raman spectroscopy of carbon-containing particles. Vib. Spectrosc. 26, 179–186. https://doi.org/10.1016/S0924-2031(01)00106-0.

Fadeel, B., Bussy, C., Merino, S., Vázquez, E., Flahaut, E., Mouchet, F., Evariste, L., Gauthier, L., Koivisto, A.J., Vogel, U., Martín, C., Delogu, L.G., Buerki-Thurnherr, T., Wick, P., Beloin-Saint-Pierre, D., Hischier, R., Pelin, M., Candotto Carniel, F., Tretiach, M., Cesca, F., Benfenati, F., Scaini, D., Ballerini, L., Kostarelos, K., Prato, M., Bianco, A., 2018. Safety assessment of graphene-based materials: focus on human health and the environment. ACS Nano 12, 10582–10620. https://doi.org/10.1021/acsnano.8b04758.

Ferrari, A.C., Robertson, J., 2000. Interpretation of Raman spectra of disordered and amorphous carbon. Phys. Rev. B 61, 14095–14107. https://doi.org/10.1103/PhysRevB.61.14095.

Garrington, A., 2020. The Graphene Market Will Reach $700m by 2031 [WWW Document]. IDTechEx. URL. https://www.idtechex.com/en/research-article/idtechex-the-graphene-market-will-reach-700m-by-2031/22414.

Genies, C., Maître, A., Lefèbvre, E., Jullien, A., Chopard-Lallier, M., Douki, T., 2013. The extreme variety of genotoxic response to benzo[a]pyrene in three different human cell lines from three different organs. PLoS One 8, e78356. https://doi.org/10.1371/journal.pone.0078356.

Hahn, J.R., 2005. Kinetic study of graphite oxidation along two lattice directions. Carbon N. Y. 43, 1506–1511. https://doi.org/10.1016/j.carbon.2005.01.032.

Health hazards of composites in fire. In: Fire Properties of Polymer Composite Materials, 2006. Springer, Netherlands, Dordrecht, pp. 359–384. https://doi.org/10.1007/978-1-4020-5356-6_12.

Hofmann, W., 2011. Modelling inhaled particle deposition in the human lung—a review. J. Aerosol Sci. 42, 693–724. https://doi.org/10.1016/j.jaerosci.2011.05.007.

Hufnagel, M., May, N., Wall, J., Wingert, N., Garcia-Käufer, M., Arif, A., Hübner, C., Berger, M., Mülhopt, S., Baumann, W., Weis, F., Krebs, T., Becker, W., Gminski, R., Stapf, D., Hartwig, A., 2021. Impact of nanocomposite combustion aerosols on A549 cells and a 3D airway model. Nanomaterials 11, 1685. https://doi.org/10.3390/nano11071685.

International Organization for Standardization, 1989. Toxicity Testing of Fire Effluents — Part 1: General.

Jonsdottir, H.R., Delaval, M., Leni, Z., Keller, A., Brem, B.T., Siegerist, F., Schönenberger, D., Durdina, L., Elser, M., Burtscher, H., Liati, A., Geiser, M., 2019. Non-volatile particle emissions from aircraft turbine engines at ground-idle induce oxidative stress in bronchial cells. Commun. Biol. 2, 1–11. https://doi.org/10.1038/s42003-019-0332-7.

Kong, W., Kum, H., Bae, S.-H., Shim, J., Kim, H., Kong, L., Meng, Y., Wang, K., Kim, C., Kim, J., 2019. Path towards graphene commercialization from lab to market. Nat. Nanotechnol. 14, 927–938. https://doi.org/10.1038/s41565-019-0555-2.

Kooter, I.M., Gröllers-Mulderij, M., Steenhof, M., Duistermaat, E., van Acker, F.A.A., Staal, Y.C.M., Tromp, P.C., Schoen, E., Kuper, C.F., van Someren, E., 2016. Cellular effects in an in vitro human 3D cellular airway model and A549/BEAS-2B in vitro cell cultures following air exposure to cerium oxide particles at an air–liquid interface. Appl. Vitr. Toxicol. 2, 56–66. https://doi.org/10.1089/aivt.2015.0030.

Kotsilkov, S., Ivanov, E., Vitanov, N., 2018. Release of graphene and carbon nanotubes from biodegradable poly(lactic acid) films during degradation and combustion: risk associated with the end-of-life of nanocomposite food packaging materials. Materials (Basel). 11, 2346. https://doi.org/10.3390/ma11122346.

Kroll, A., Pillukat, M.H., Hahn, D., Schnekenburger, J., 2012. Interference of engineered nanoparticles with in vitro toxicity assays. Arch. Toxicol. 86, 1123–1136. https://doi.org/10.1007/s00204-012-0837-z.

Laachachi, A., Burger, N., Apaydin, K., Sonnier, R., Ferriol, M., 2015. Is expanded graphite acting as flame retardant in epoxy resin? Polym. Degrad. Stab. 117, 22–29. https://doi.org/10.1016/j.polymdegradstab. 2015.03.016.

Leibrock, L.B., Jungnickel, H., Tentschert, J., Katz, A., Toman, B., Petersen, E.J., Bierkandt, F.S., Singh, A.V., Laux, P., Luch, A., 2020. Parametric optimization of an air–liquid interface system for flow-through inhalation exposure to nanoparticles: assessing dosimetry and intracellular uptake of CeO2 nanoparticles. Nanomater. https://doi.org/10.3390/nano10122369.

Levchik, S.V., Weil, E.D., 2004. Thermal decomposition, combustion and flame-retardancy of epoxy resins-a review of the recent literature. Polym. Int. 53, 1901–1929. https://doi.org/10.1002/pi.1473.

Li, Y., Liu, Y., Fu, Y., Wei, T., Le Guyader, L., Gao, G., Liu, R.-S., Chang, Y.-Z., Chen, C., 2012. The triggering of apoptosis in macrophages by pristine graphene through the MAPK and TGF-beta signaling pathways. Biomaterials 33, 402–411. https://doi.org/10.1016/j.biomaterials.2011.09.091.

Liu, S., Yan, H., Fang, Z., Wang, H., 2014. Effect of graphene nanosheets on morphology, thermal stability and flame retardancy of epoxy resin. Compos. Sci. Technol. 90, 40–47. https://doi.org/10.1016/j.compscitech.2013.10.012.

Liu, S., Fang, Z., Yan, H., Chevali, V.S., Wang, H., 2016. Synergistic flame retardancy effect of graphene nanosheets and traditional retardants on epoxy resin. Compos. Part A Appl. Sci. Manuf. 89, 26–32. https://doi.org/10.1016/j.compositesa.2016.03.012.

Motzkus, C., Chivas-Joly, C., Guillaume, E., Ducourtieux, S., Saragoza, L., Lesenechal, D., Macé, T., 2011. Characterization of aerosol emitted by the combustion of nanocomposites. J. Phys. Conf. Ser. 304, 012020 https://doi.org/10.1088/1742-6596/304/1/012020.

Netkueakul, W., Fischer, B., Walder, C., Nüesch, F., Rees, M., Jovic, M., Gaan, S., Jacob, P., Wang, J., 2020a. Effects of combining graphene nanoplatelet and phosphorous flame retardant as additives on mechanical properties and flame retardancy of epoxy nanocomposite. Polymers (Basel). 12, 2349. https://doi.org/10.3390/polym12102349.

Netkueakul, W., Korejwo, D., Hammer, T., Chortarea, S., Rupper, P., Braun, O., Calame, M., Rothen-Rutishauser, B., Buerki-Thurnherr, T., Wick, P., Wang, J., 2020b. Release of graphene-related materials from epoxy-based composites: characterization, quantification and hazard assessment in vitro. Nanoscale 12, 10703–10722. https://doi.org/10.1039/C9NR10245K.

Nisbet, I.C.T., LaGoy, P.K., 1992. Toxic equivalency factors (TEFs) for polycyclic aromatic hydrocarbons (PAHs). Regul. Toxicol. Pharmacol. 16, 290–300. https://doi.org/10.1016/0273-2300(92)90009-X.

Ohtoshi, T., Takizawa, H., Okazaki, H., Kawasaki, S., Takeuchi, N., Ohta, K., Ito, K., 1998. Diesel exhaust particles stimulate human airway epithelial cells to produce cytokines relevant to airway inflammation in vitro. J. Allergy Clin. Immunol. 101, 778–785. https://doi.org/10.1016/S0091-6749(98)70307-0.

Ou, L., Song, B., Liang, H., Liu, J., Feng, X., Deng, B., Sun, T., Shao, L., 2016. Toxicity of graphene-family nanoparticles: a general review of the origins and mechanisms. Part. Fibre Toxicol. 13, 57. https://doi.org/10.1186/s12989-016-0168-y.

Park, E.J., Lee, S.J., Lee, K., Choi, Y.C., Lee, B.S., Lee, G.H., Kim, D.W., 2017. Pulmonary persistence of graphene nanoplatelets may disturb physiological and immunological homeostasis. J. Appl. Toxicol. 37, 296–309. https://doi.org/10.1002/jat.3361.

Reiss, T., Hjelt, K., Ferrari, A.C., 2019. Graphene is on track to deliver on its promises. Nat. Nanotechnol. 14, 907–910. https://doi.org/10.1038/s41565-019-0557-0.

Reuter, S., Gupta, S.C., Chaturvedi, M.M., Aggarwal, B.B., 2010. Oxidative stress, inflammation, and cancer: How are they linked? Free Radic. Biol. Med. 49, 1603–1616. https://doi.org/10.1016/j.freeradbiomed.2010.09.006.

Schinwald, A., Murphy, F.A., Jones, A., MacNee, W., Donaldson, K., 2012. Graphene-based nanoplatelets: a new risk to the respiratory system as a consequence of their unusual aerodynamic properties. ACS Nano 6, 736–746. https://doi.org/10.1021/nn204229f.

Schmittgen, T.D., Livak, K.J., 2008. Analyzing real-time PCR data by the comparative CT method. Nat. Protoc. 3, 1101–1108. https://doi.org/10.1038/nprot.2008.73.

Shimada, T., Fujii-Kuriyama, Y., 2004. Metabolic activation of polycyclic aromatic hydrocarbons to carcinogens by cytochromes P450 1A1 and1B1. Cancer Sci. 95, 1–6. https://doi.org/10.1111/j.1349-7006.2004.tb03162.x.

Shimada, T., Guengerich, F.P., 2006. Inhibition of human cytochrome P450 1A1-, 1A2-, and 1B1-mediated activation of procarcinogens to genotoxic metabolites by polycyclic aromatic hydrocarbons. Chem. Res. Toxicol. 19, 288–294. https://doi.org/10.1021/tx050291v.

Shiomi, A., Usui, T., 2015. Pivotal roles of GM-CSF in autoimmunity and inflammation. Mediat. Inflamm. 2015, 1–13. https://doi.org/10.1155/2015/568543.

Singh, D., Schifman, L.A., Watson-Wright, C., Sotiriou, G.A., Oyanedel-Craver, V., Wohlleben, W., Demokritou, P., 2017. Nanofiller presence enhances polycyclic aromatic hydrocarbon (PAH) profile on nanoparticles released during thermal decomposition of nano-enabled thermoplastics: potential environmental health implications. Environ. Sci. Technol. 51, 5222–5232. https://doi.org/10.1021/acs.est.6b06448.

Vejerano, E.P., Holder, A.L., Marr, L.C., 2013. Emissions of polycyclic aromatic hydrocarbons, polychlorinated dibenzo- p -dioxins, and dibenzofurans from incineration of nanomaterials. Environ. Sci. Technol. 47, 4866–4874. https://doi.org/10.1021/es304895z.

Wang, S., Tambraparni, M., Qiu, J., Tipton, J., Dean, D., 2009. Thermal expansion of graphene composites. Macromolecules 42, 5251–5255. https://doi.org/10.1021/ma900631c.

Wang, J., Chen, Z., Chen, B., 2014. Adsorption of polycyclic aromatic hydrocarbons by graphene and graphene oxide nanosheets. Environ. Sci. Technol. 48, 4817–4825. https://doi.org/10.1021/es405227u.

Watson-Wright, C., Singh, D., Demokritou, P., 2017. Toxicological implications of released particulate matter during thermal decomposition of nano-enabled thermoplastics. NanoImpact 5, 29–40. https://doi.org/10.1016/j.impact.2016.12.003.

Welch, J., Wallace, J., Lansley, A.B., Roper, C., 2021. Evaluation of the toxicity of sodium dodecyl sulphate (SDS) in the MucilAirTM human airway model in vitro. Regul. Toxicol. Pharmacol. 125, 105022 https://doi.org/10.1016/j.yrtph.2021.105022.

Wick, P., Louw-Gaume, A.E., Kucki, M., Krug, H.F., Kostarelos, K., Fadeel, B., Dawson, K. A., Salvati, A., Vázquez, E., Ballerini, L., Tretiach, M., Benfenati, F., Flahaut, E., Gauthier, L., Prato, M., Bianco, A., 2014. Classification framework for graphene-based materials. Angew. Chem. Int. Ed. 53, 7714–7718. https://doi.org/10.1002/anie.201403335.

Xiao, L., Zheng, Z., Irgum, K., Andersson, P.L., 2020. Studies of emission processes of polymer additives into water using quartz crystal microbalance—a case study on organophosphate esters. Environ. Sci. Technol. 54, 4876–4885. https://doi.org/10.1021/acs.est.9b07607.

Yang, K., Li, Y., Tan, X., Peng, R., Liu, Z., 2013. Behavior and toxicity of graphene and its functionalized derivatives in biological systems. Small 9, 1492–1503. https://doi.org/10.1002/smll.201201417.

Yu, B., Shi, Y., Yuan, B., Qiu, S., Xing, W., Hu, W., Song, L., Lo, S., Hu, Y., 2015. Enhanced thermal and flame retardant properties of flame-retardant-wrapped graphene/epoxy resin nanocomposites. J. Mater. Chem. A 3, 8034–8044. https://doi.org/10.1039/C4TA06613H.

Zhang, X.F., Xi, Q., 2011. A graphene sheet as an efficient electron acceptor and conductor for photoinduced charge separation. Carbon N. Y. 49, 3842–3850. https://doi.org/10.1016/j.carbon.2011.05.019.

Zhang, B., Wei, P., Zhou, Z., Wei, T., 2016. Interactions of graphene with mammalian cells: molecular mechanisms and biomedical insights. Adv. Drug Deliv. Rev. 105, 145–162. https://doi.org/10.1016/j.addr.2016.08.009.

Zhang, Q., Wang, Y.C., Bailey, C.G., Yuen, R.K.K., Parkin, J., Yang, W., Valles, C., 2018. Quantifying effects of graphene nanoplatelets on slowing down combustion of epoxy composites. Compos. Part B Eng. 146, 76–87. https://doi.org/10.1016/j.compositesb.2018.03.049.